

AIAA '89

AIAA
TP
89-1040

A89-40469

AIAA-89-1040

**Determination of Near and Far Field Acoustics
for Advanced Propeller Configurations**
K.D. Korkan, S.M. Jaeger and J.H. Kim
Texas A&M University, College Station, TX

1989 JUN 16 10:00

AIAA 12th Aeroacoustics Conference

April 10-12, 1989 / San Antonio, TX

V

DETERMINATION OF NEAR AND FAR FIELD ACOUSTICS FOR ADVANCED PROPELLER CONFIGURATIONS

K.D. Korkan*, S.M. Jaeger** and J.H. Kim**
Texas A&M University
College Station, Texas

A89-40469

Abstract

A method has been studied for predicting the acoustic field of the SR-3 transonic propfan using flow data generated by two versions of the NASPROP-E computer code. Since the flow field(s) calculated by the solver(s) include the shock wave system of the propeller, the nonlinear quadrupole noise source term is included along with the monopole and dipole noise sources in the calculation of the acoustic near field. Acoustic time histories in the near field are determined by transforming the azimuthal coordinate in the rotating, blade fixed coordinate system to the time coordinate in a non-rotating coordinate system. Fourier analysis of the pressure time histories is used to obtain the frequency spectra of the near field noise. The method is used to investigate the effects of boundary condition reflection, artificial viscosity, and azimuthal grid spacing on the near field acoustic time histories and frequency spectra at preselected observer locations. Acoustic characteristics in the far field are investigated by applying Kirchoff's theorem to a non-rotating control surface about the propeller configuration as proposed by Farassat. The method utilizes near field acoustic pressure data as a function of time and location as provided by the flow field solvers.

Nomenclature

a_k	Fourier cosine coefficient for kth harmonic
a_o	speed of sound
b	radius of control cylinder in far field method
b_k	Fourier sine coefficient for nth harmonic
C	control surface for far field analysis
CFL	Courant-Friedrichs-Lowy number
f	surface of body in motion
J	grid index for the axial direction
J_m	Bessel function of the mth order
K	grid index for the radial direction
L	grid index for the azimuthal direction
m	harmonic number
M_r	component of Mach number in \hat{r} direction
M_n	normal component of Mach number
M_t	tangential component of Mach number
\bar{M}	Mach number vector
\hat{n}	outward vector normal to C

P', P	acoustic pressure at a point
P_{ref}	acoustic reference pressure, 20 μ Pascals
P_{rms}	root-mean-squared pressure
r	radial coordinate in cylindrical coordinates
\hat{r}	radiation vector
R	distance from source to observer
R_o	distance from origin to observer
ret	retarded time
S	control surface for far field analysis
t	observer time
T	period
U	axial velocity of propeller
V	control volume
x_i	point in Cartesian coordinates
\underline{x}	observer location
z	axial coordinate in cylindrical coordinates
ϕ	azimuthal coordinate in cylindrical coord.
ζ	azimuthal coordinate in body-fitted coord.
η	radial coordinate in body-fitted coordinates
ξ	axial coordinate in body-fitted coordinates
Ω	rotational speed of propeller
ρ_o	freestream density
μ, ν	spherical coordinates as shown in Fig. 13
τ	source time
Φ	velocity potential (acoustic pressure)
θ	angle between \hat{r} and \hat{n}

Introduction

The prospect of rising fuel costs has generated new interest in propeller technology. Propellers in the past were efficient at lower speeds, but the propulsive efficiency of traditional propellers decreases rapidly with increasing Mach number. As a result, these propulsion devices were unable to compete economically at higher speeds associated with modern commercial jets. However, the turbojets and turbofans presently used are more efficient when operating at higher Mach numbers than used presently for jet transports. An intermediate propulsion concept is needed to properly fill the speed range between the propeller and turbofan.

One possible propulsion concept for the high subsonic speed regime is the transonic propfan. With six to ten thin, highly swept blades, and high disk loading, the propfan represents the middle ground between the turbofan and the traditional propeller. These properties present new problems in acoustic analyses since methods presently in use do not account for these effects. Noise associated with propellers contains acoustic power at a specific set of frequencies which are harmonics of the blade passing frequency. Propfans may produce exces-

* Professor, Aerospace Engineering Department, Associate Fellow AIAA

** Graduate Research Assistant, Aerospace Engineering Department, Student Member AIAA

sive noise levels compared to the noise of a conventional propeller, which is chiefly due to the presence of local supersonic flow and shock waves in the tip region of the propfan. Excessive near field noise results in high cabin acoustic values, and over a period of time may possibly cause acoustic structural fatigue. Knowledge of the flow field and the acoustic field produced by the propfan is necessary to effectively address these problems.

For a propeller operating in the transonic range, there are three mechanisms by which propeller noise is produced. Noise which is the result of the periodic volumetric displacement of air by the propeller, has the character of an acoustic monopole^{1,2}. Noise which arises from the periodic translational displacement of air due to the resultant aerodynamic forces acting on the blade has the character of an acoustic dipole. When shock waves or regions of extreme gradients are present, a third mechanism produces noise with the nature of an acoustic quadrupole. Unlike monopole and dipole noise sources which radiate from the propeller blade surface, quadrupole noise sources radiate from any region in the flow field where shock waves or extreme flow gradients are present. These noise mechanisms have been identified mathematically in the Ffowcs Williams-Hawkings equation² as described by Farassat³.

A flow field solution which accounts for the presence of shock waves in addition to the monopole and dipole effects is needed to accurately model the acoustic properties of the transonic propfan. A tip shock wave on a propeller is a nonlinear mechanism which produces significant levels of the quadrupole source. In propellers with subsonic tip speeds, the strength of the quadrupole noise source is negligibly small, and the use of linear acoustic analysis is appropriate. As a result, most methods developed in the past have neglected the quadrupole noise source term in their theoretical development³. With the advent of the propfan however, quadrupole sources must be included since the non-linear quadrupole noise at supersonic tip speeds is a significant contributor to overall noise levels.

Review of Acoustic Prediction Methods

The first significant contributions made in the theoretical prediction of propeller noise were those of Lynam and Webb⁴ in 1919 and Hart⁵ in 1930. However, these methods failed to produce proper directivity patterns of the predicted noise levels. In 1936, Gutin⁶ developed a method which was based on the aerodynamic loading distribution on the propeller disk. Gutin's theory is still valid in the near field case, and using this method Hubbard and Regier⁷ were able to correlate well with experimental values. Gutin's theory was extended further by Garrick and Watkins⁸ to include the effects of forward motion of the propeller on the acoustic field.

In 1952 Lighthill¹ published his theory of aerodynamic sound which included the effects of volumetric displacement, resultant aerodynamic forces, and external fluid stresses as acoustic monopole, dipole and

quadrupole noise sources. The Lighthill acoustic analogy was extended by Ffowcs Williams and Hawkings² by the use of generalized functions which facilitate the evaluation of integrals which may have singularities that render other solution methods impractical. Hawkings and Lawson⁹ developed a far field method for planar rotors in a static environment which can calculate the monopole and dipole noise components for both subsonic and supersonic tip speeds. The frequency spectrum is calculated for a set of noise sources which are fixed to the propeller blades rotating in a fluid fixed coordinate system. Jou¹⁰ extended this method to the forward flight case and modified the formulation using a planar disk of fixed periodic sources rather than a set of rotating constant sources.

Farassat's method¹¹ can be used in both near and far field for a general propeller geometry and motion as in forward flight. Farassat applies the collapsing sphere method by dividing the propeller blades into panels and then further subdividing the set of source panels on the blade into subsonic and supersonic regions. Results from Farassat and Succi¹² and Nystrom and Farassat¹³ for various geometries and operating conditions show that this method can predict proper acoustic behavior when the propeller tip region is not expected to produce strong shock waves. However, it is believed that the exclusion of the non-linear quadrupole source in the higher speed cases resulted in underprediction of acoustic values in the lower harmonics^{12,13}. In a recent study, Farassat proposes a method which includes the effects of quadrupole sources in shock waves, boundary layers and wake sources¹⁴. The collapsing sphere method is also used in the time domain solution by Hanson¹⁵. Hanson also has developed a frequency domain solution method employing a Fourier transform applied to the Ffowcs-Williams Hawkings equation for a non-rotating coordinate system¹⁶. Woan and Gregorek¹⁷ assumes steady blade loading and subsonic tip speeds. In comparisons with experimental data, this method has been shown to accurately predict acoustic values for standard turboprop propellers¹⁸. Succi¹⁹ also assumes steady loading and subsonically moving sources, but also assumes the thickness and loading sources are compact segments rather than chordwise distributions.

All of the methods mentioned previously do not include the non-linear quadrupole noise source term as contained in the Ffowcs Williams-Hawkings equation. However, Hanson and Fink²⁰ have formulated a method for an unloaded rotor operating in a static environment. In general, linear acoustic prediction methods have been sufficiently accurate to allow designers of propellers to determine the noise levels for low Mach number applications. However, the transonic propfan operates at high subsonic Mach numbers with highly loaded blades in which the propeller tips travel at supersonic speeds. Complete solutions of the Ffowcs Williams-Hawkings equation including the nonlinear volume integrals may require excessive computational effort compared to that

of linear solution schemes.

The present approach uses a three dimensional Euler analysis to account for the non-linear effects of supersonic flow for a large domain on and around the propeller and nacelle. Acoustic analysis is applied to any point within the computational domain thereby in effect accounting for the monopole, dipole, and quadrupole noise source terms to obtain acoustic pressure time histories and frequency spectra for a given flow solution. This eliminates the need to explicitly solve Lighthill's equation.

Present Approach

In this study, the non-linear character of the flow field is accounted for by the use of the NASPROP-E computer code. This program solves the three-dimensional Euler equations in weak conservation law form in the coordinate system shown in Fig. 1 using an implicit finite difference approximate factorization scheme^{21,22}. The solution method models the inviscid non-linear behavior in the propeller flow field including shock waves and tip vortices. This Beam Warming type solution is weakly unstable in three dimensions and artificial dissipation must be added to obtain a converged solution. The governing equations are cast in cylindrical coordinates (z, r, θ) and then transformed into body-fitted coordinates spinner and nacelle of the SR-3 are both axisymmetric, the flow field can be assumed to be periodic for one blade passage. The nacelle and spinner are mapped onto the first constant η surface and the inflow/freestream boundary is mapped on the last surface which is placed approximately three diameters away from the propeller. The suction surface of the blade is mapped onto the first constant ζ boundary and the compression surface is mapped onto the last constant ζ boundary. The remaining region of both the first and last constant ζ boundary constitute the periodic boundaries. For the SR-3 geometry there are eight blades, therefore these boundaries are separated by an angle of 45° . The first constant ξ surface collapses into the upstream stagnation streamline on the propeller axis and the last constant ξ surface is the outflow boundary which is placed two diameters downstream of the propeller.

The conditions applied at each of the boundaries are the analog of a propeller operating in an infinite fluid which is assumed to be an inviscid, calorically perfect, and non-heat conducting medium. The freestream boundary is updated using Riemann invariants in the non-reflecting version of the computer analysis. The reflecting version maintains constant freestream conditions for all time steps at this boundary. The outflow boundary specifies the exit pressure by integrating the radial pressure gradient calculated from the radial equilibrium equation. Flow tangency is enforced on the solid surface boundaries by a separate explicit scheme.

The flow field solutions generated in the following segments are compared to a common case using

the non-reflecting boundary conditions in a smoothed grid with 45 axial, 21 radial and 21 azimuthal coordinate stations. Solutions of the transonic flow field were obtained using a Courant number of 4.0 and run for 10,000 iterations using explicit fourth-order and implicit second-order damping of 4.0 and 8.0, respectively. The user-defined variables of azimuthal mesh spacing and damping as well as the free-stream boundary conditions were varied independent of each other in the comparisons presented. The Courant number and number of iterations were kept fixed for all cases, and the L_2 norm of the residual dropped by approximately three orders of magnitude for convergence.

Previous studies²³⁻²⁵ have shown that the acoustic near field overall sound pressure level (OASPL) can be obtained by the integration of the pressures at a specified radial distance from the axis of rotation using a root-mean-square method. The OASPL at a given point is found by transforming ϕ , the azimuthal coordinate in the rotating coordinate system of the flow solver into t , the observer time in stationary coordinates by using the relation, $t = d/l$, where l is the rotational speed of the propeller. Therefore, to obtain OASPL:

$$OASPL = 10 \log_{10} \left[P_{rms}^2 / P_{ref}^2 \right] \quad (1)$$

using a reference pressure of 20μ Pa. Also, P_{rms} is defined by the expression:

$$P_{rms}^2 = 1/(T_2 - T_1) \int_{T_1}^{T_2} P^2(t) dt \quad (2)$$

where $P(t)$ is the acoustic or perturbation pressure. The frequency spectra can be obtained by using the Fourier series representation of the acoustic pressure time-history calculated from the flow field solver²³⁻²⁵. The Fourier coefficients, a_k and b_k , calculated by trapezoidal rule integration, are given by:

$$P_{rms}^2 = \frac{1}{2} \sum_{k=1}^{\infty} (a_k^2 + b_k^2) \quad (3)$$

where the SPL of the k th harmonic of the fundamental frequency is given as:

$$SPL = 10 \log_{10} \left[(a_k^2 + b_k^2) (\sqrt{2} P_{ref}) \right]^2 \quad (4)$$

The acoustic solution can then properly account for the same non-linear effects in the near field as those of the flow field solver. Using this approach, Korkan, et. al.^{24,25} and White²³ have reached good agreement with the experimental data of Dittmar, et. al.^{26,27} for the SR-3 propfan configuration at a freestream Mach Number of 0.80.

In the present study, the influence of grid spacing, inflow/freestream boundary conditions, and artificial damping of the Euler solver on the acoustic solu-

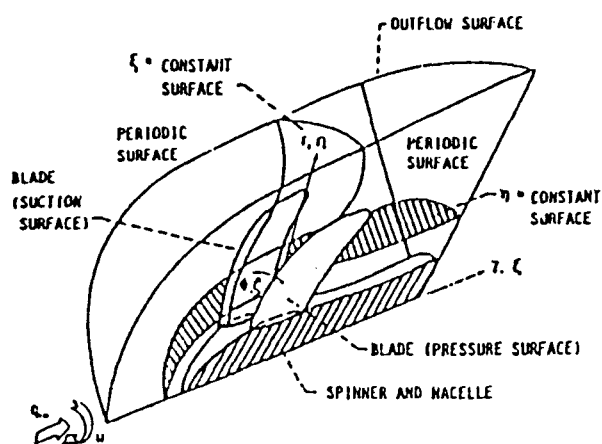


Figure 1. Near Field Method Coordinate System.

tions of the near field have been examined by using three different grids, two different sets of inflow/free-stream boundary conditions, and four different damping values. Problems in generating the transonic flow field were encountered in the studies previously mentioned²³⁻²⁵ since the above parameters could not always be varied independently while still obtaining a converged solution.

The near field solution is limited to points well within the computational domain. Points near the inflow and outflow boundaries typically do not give good results due to the coarse computational mesh spacing in this region and/or reflective interference due to the type of boundary conditions in the solution method. In addition, acoustic information for points outside the computational mesh must be calculated. Here, in the acoustic far field, the data from the flow field solver can be used to calculate the acoustic perturbation pressure at a given observer location by applying Kirchhoff's theorem in the integration of flow field data on a control cylinder which encloses the shock wave system of the propeller. Outside of this control cylinder, linear wave propagation theory can be applied to obtain the solution either in the time or frequency domain²⁶⁻³⁰. It is important to note that the manner in which the data for the flow field is obtained is not crucial and that both methods could be adapted to any non-linear solution method. Any solution scheme that accurately models the flow field around the propeller, or even experimental flow measurements, may be used for both near and far field methods using the present theoretical approach.

Effects of Azimuthal Mesh Spacing

In order to determine whether the quality of the acoustic data generated by the flow solver can be improved by modification of the computational mesh, the high aspect ratio grid cells in the disk plane region beyond the propeller tip were smoothed. Further, the

number of grid points in the azimuthal blade to blade direction has been increased from 11 to 21, and then 41 points. A finer mesh in the blade-to-blade direction is expected to better resolve the shock wave structure, produce finer detail in the acoustic time-history, and to provide more data points for Fourier analysis in calculating frequency spectra.

In this study, the non-reflecting version of NASPROP-E generated the flow fields, and the radial-axial planes of the computational domain remained approximately the same. Radially, there were 12 stations from the nacelle/spinner to the tip with the remaining 9 stations extending to the inflow boundary. Axially, the first 14 stations are upstream of the propeller, the 15th through the 30th represent the blade region from the leading to the trailing edge, and the 31st to the 45th are the aft or wake region of the mesh. The flow fields for the grid comparison were generated using a Courant number of 4.0 with implicit and explicit damping values of 4.0 and 8.0, respectively.

The refinement of the mesh for this study involved two phases. The first phase addressed the problem of excessive grid point clustering in the acoustic near field region in the propeller disk plane. This was an attempt to address grid dependence on the acoustic directivity pattern as shown by White²³. The second phase was to increase the azimuthal mesh spacing from 11 to 21 and then to 41 computational points to see the effect of the refinement on the acoustic pressure time history. This was an attempt to address the more basic problem of the time accuracy of the acoustic data and the ability of the method to properly predict the harmonic content of the acoustic signal.

In order to solve the problem of excessive grid point clustering in the radial/axial planes of the grid, a simple iterative smoothing scheme was used. Each point in the domain that was not on a solid surface was moved according to a weighted linear average of the positions of its eight nearest neighbors in the same radial/axial plane. The weighting factors controlled the rates of smoothing in both the radial and axial directions. The desired result was to increase the mesh spacing in the axial direction for the region in the disk plane which is beyond the propeller blade tip as shown in Fig. 2. These results were obtained by setting the radial smoothing rate to zero so that the expansion of the grid would occur in the axial direction only. Although the flow fields generated in the smoothed domain still show the effects of grid dependence, the radial/axial grid refinement results in a more realistic directivity pattern as shown in Fig. 3.

In order to evaluate the effects of azimuthal grid refinement, flow fields were generated using grids with 11, 21, and 41 azimuthal planes. With the exception of the pressure time history at the location J=12, K=14, significant differences appear in the acoustic pressure time histories as the number of azimuthal grid points is increased from 11 to 21 points for the two radial stations

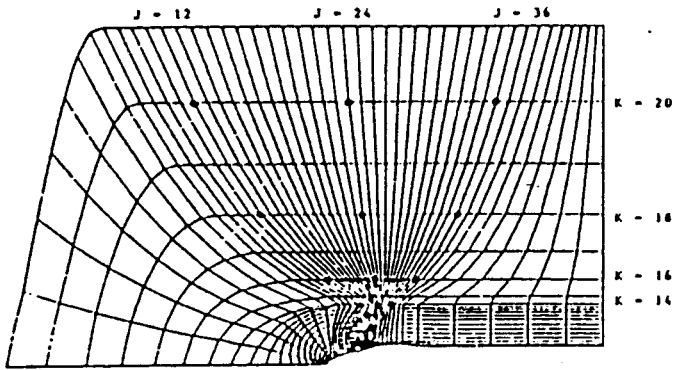


Figure 2. Smoothed Azimuthal Grid Plane for Near Field.

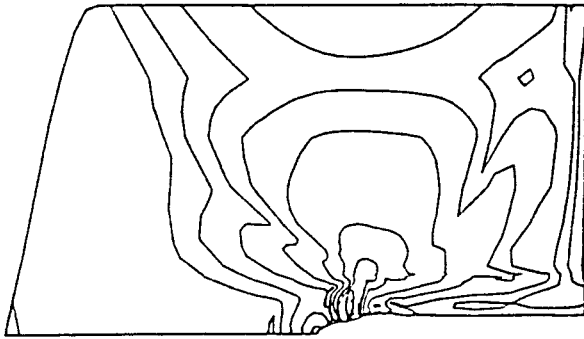


Figure 3. OASPL Directivity Pattern for Smoothed Grid.

nearest the blade tip ($K=14$ and 16). The additional resolution in the pressure time-histories is shown in the increase in detail and the appearance of additional features in the pressure and suction peaks as seen in Fig. 4. For the two radial stations further from the blade tip corresponding to $K=18$ and $K=20$, the greatest change still occurs as the azimuthal points are increased from 11 to 21, however the acoustic waveforms generated in all three grids are similar than those occurring near the propeller.

For all points used in the acoustic calculations, the similarities between the 21 and 41 point results are also evident in the first three harmonics of the frequency spectra as seen in Fig. 5. Problems are encountered in predicting the higher harmonics of the acoustic signal. Although the azimuthal mesh spacing for the 41 point grid is very fine for performance calculations, a 41 point acoustic pressure time history is still considered to be very coarse. The highest harmonic that can be calculated from a data set of N data points is less than or equal to $N/2$. Note that for the 11 point grid only the first 5 harmonics are shown in the frequency spectra. The limiting values for the 21 and 41 point waveforms

are 10 and 20, respectively. Even if it is possible to calculate the higher harmonics from the raw data, the quality of that data can be affected by the distribution of grid points between the noise sources and the observer point.

An additional effect of azimuthal grid refinement was a loss of stability in the solution of the propeller flow field. It was determined that as the number of grid points increase, the amount of dispersive waves in the Mach contours also increases. This result is expected since the effect of the damping is proportional to the local time step for a fixed CFL number. Therefore, as the mesh spacing decreases, the effect of the damping also decreases. However, this problem is not as important as the distribution of grid points since the damping values can be adjusted globally. The more difficult problem is adjusting the grid so the solution scheme properly models the physics of the flow in the largest continuous region possible.

The critical point is that the region of interest for performance calculations, the task which the Euler solvers are intended for, is almost entirely within the propeller disk and the propeller wake immediately downstream of the propeller. The region of interest for near field acoustics is significantly larger than the propeller radius and also includes the regions upstream and downstream of the propeller. Although proper application of the far field method may reduce the size of the computational region needed for accurate near field acoustic treatment, it is likely that the major limitation of this method may be the product of near field grid spacing rather than boundary condition reflections or non-uniform damping.

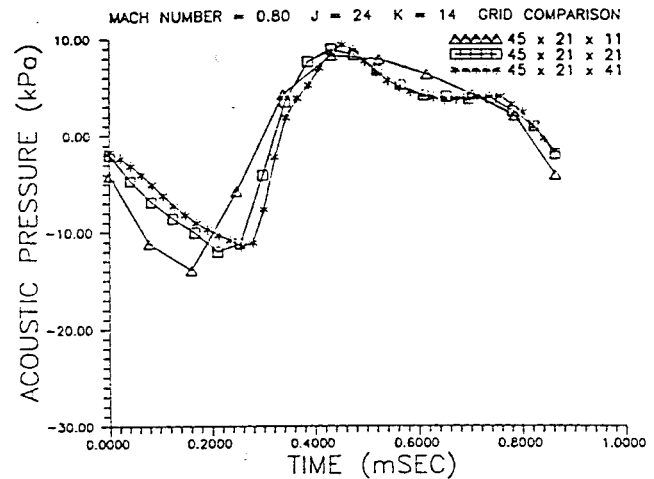


Figure 4. Acoustic Pressure Time-Histories for Three Grids. $r/R_{tip} = 1.08$ $z/R_{tip} = 0.25$

Effects of Boundary Condition Reflection

The study of inflow and outflow boundary conditions for a flow field solution involves the means by

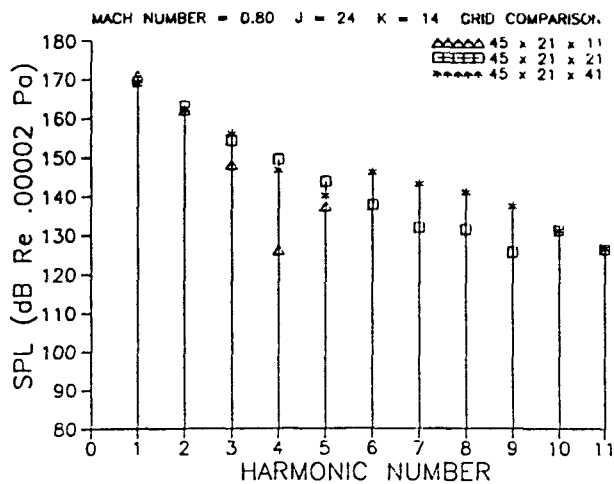


Figure 5. Frequency Spectra for Three Grids.
 $r/R_{tip} = 1.08$ $z/R_{tip} = 0.25$

which the freestream conditions in a fluid of infinite extent are modelled in a limited computational domain. Computational time and memory space limitations make it impractical to use a large grid extending far from the region of interest around the propeller. The two methods used to resolve the problem of limited space are either to transform the infinite physical space into a finite computational space, or to enforce flow conditions at a computational boundary at some finite distance which is an approximation of the conditions that would result from having an infinite computational domain. For the solution of the potential equation, the coordinate transformation technique is most commonly used. However in the solution of the Euler equations, the mapping method is not as easily applied. As a result, most Euler solvers use the approximation method for a finite domain.

The effects of two different approximation methods are seen in the present study. Both versions of NASPROP-E solve the Euler equations in a "conical" curvilinear coordinate system. The conical segment of the outer surface of the mesh constitutes the inflow boundary, and the base of the cone downstream of the propeller is the outflow boundary. Since the nacelle is axisymmetric and the disk plane is normal to the freestream, the flow field is assumed periodic between any two adjacent blades. Therefore, only one "slice" between two blades need be solved, and the periodic surface defines the boundaries of the slice. The reflecting version of NASPROP-E uses constant freestream conditions for the inflow boundary. This means the flow variables at the boundary are initialized to freestream conditions and remain unchanged for all subsequent time steps, since the main iteration scheme never updates the points on the inflow surface. The non-reflecting version calculates the inflow variables by using Riemann invariants to obtain the local speed of sound and the velocity component normal to the boundary. The tangen-

tial velocity component and the entropy toggle between freestream values for velocity influx at the boundary and values extrapolated from the interior for velocity efflux at the boundary. Both versions solve implicitly the periodic system of equations for the periodic boundary, and a simplified version of the radial equilibrium equation is used to obtain the radial pressure gradient which is integrated using trapezoidal rule from the outer edge to the nacelle.

The significance of the comparison of the two approaches is that the boundaries solved using the fixed static pressure are more reflective than the boundaries solved by Riemann invariants. To effectively use Euler analysis to obtain acoustic data, the reflectiveness of the inflow/outflow boundary should be minimized since excessive numerical reflection is likely to contaminate the acoustic solution in both the near and far field.

The acoustic data was calculated for the eight-blade SR-3 propeller with a blade angle of 57.90° and an advance ratio of 3.06 in an attempt to reproduce the experimental conditions of Dittmar^{26,27}. The freestream Mach number used for all calculations was 0.80. For regions near the blade tip corresponding to $K=14$ and 16, the effect of boundary conditions cannot be seen on either the pressure time histories or the frequency spectra. For the next radial location away from the blade which has a K value of 18, the effect of the change in boundary conditions begins to become apparent in the pressure time-histories, but not in the frequency spectra. The last radial station ($K=20$) is directly adjacent to the inflow/freestream boundary and it is here that the effects of the reflecting/non-reflecting boundary condition(s) becomes most apparent as shown in Fig. 6. The change from reflective to non-reflective boundary conditions manifests itself as a decrease in the amplitude of the acoustic waveform at a given point near the boundary of the computational domain. This is expected since the reflecting boundary conditions are analogous to a solid wall boundary with fixed freestream conditions. One should also note that the greatest change in the acoustic waveform resulting from the differing boundary conditions is greater in the downstream direction. This effect may be partially due to the proximity of the outflow boundary.

When this method was first developed, it was believed that reflections resulting from the external boundary conditions would be a large source of error in the acoustic analysis. The results of the present study show that this is not the case. Compared to the effects of grid spacing and numerical damping, the effects of boundary reflections are extremely small and appear to be restricted to the coarse regions in the grid that are far from the propeller to be expected to yield good acoustic data.

Effects of Artificial Viscosity

In the solution scheme used to obtain the pro-

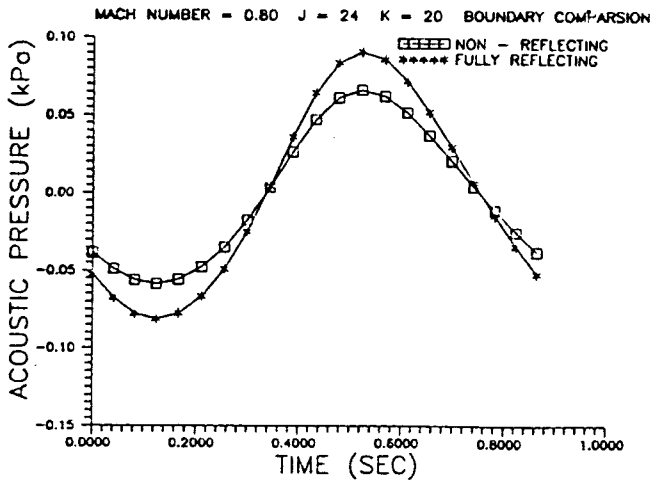


Figure 6. Acoustic Pressure Time-Histories for Different Inflow Boundaries. $r/R_{tip} = 4.66$ $z/R_{tip} = -0.24$

propeller flowfields, the 2nd and 4th order smoothing coefficients must be specified by the user and must be chosen such that transient oscillations and dispersive waves will not be amplified as the time stepping scheme progresses. Since flowfield solutions obtained using different amounts of smoothing can exhibit different flow behavior, it is important to know how these differences affect the predicted acoustic signature. The damping comparison matrix used the 45-21-21 smoothed grid, non-reflecting inflow boundary conditions, and a Courant number of 4.0 for all cases. Originally, three flowfields were generated with explicit/implicit damping factors of 8.00/16.00, 4.00/8.00, and 2.00/4.00. It was later found that the two larger damping cases were still too highly damped in the region used for the acoustic calculations. An attempt was made to find the solution scheme stability limit for low damping for the given grid, Courant number and propeller operating conditions. Additional cases were run for damping of 1.50/3.00 and 1.75/3.50 in which the lower damping case failed to converge. The remaining four flow solutions were used to generate the acoustic data presented in the damping comparison.

The effect of the variation of damping on the acoustic solution appears to have a strong dependence on the observer location in the computational domain. For the radial station closest to the propeller disk, i.e. $K=14$, phase shifts in the pressure time histories can be observed in the upstream station ($J=12$). For the observer point directly off the blade tip which is $K=14$, $J=24$, the expected result of decreased damping is apparent. The bottom of the suction peak is sharper, the compression wave is steeper and higher, and some oscillation can be seen after the pressure peak in the two lowest damping cases as shown in Fig. 7. For the point downstream of the blade tip ($K=14$, $J=36$), the suction peak is sharper for the lower damping cases. However, the compression wave is steeper and higher for the higher damping

cases. For each of the three axial stations shown for $K=14$, the frequency spectra show the expected increase in the magnitude of the higher harmonics with decreasing damping as given in Fig. 8. For the next radial station away from the tip, the most significant trend that can be seen in the acoustic pressure time histories is the forward phase shift with decreasing damping. For the 8.00/16.00 damping solution at $K=16$, $J=12$, it is difficult at first to determine if it is phase shifted forward or backward. Given the magnitude of the apparent shift of the 4.00/8.00 solution at the same point, the conclusion is that the 8.00/16.00 waveform has shifted backward sufficiently far that the pressure peak has been shifted through the periodic boundary. The increase in the magnitude of the higher harmonics resulting from lower damping are still apparent at $K=16$, although the increase is not as great as shown at $K=14$. For the two radial stations furthest from the tip ($K=18$ and $K=20$), the phase shift phenomena is still apparent. In addition, the amplitude of the acoustic waves is decreasing with the level of damping. The frequency spectra from these locations also show a decrease in SPL for the fundamental and higher harmonics with decreasing damping.

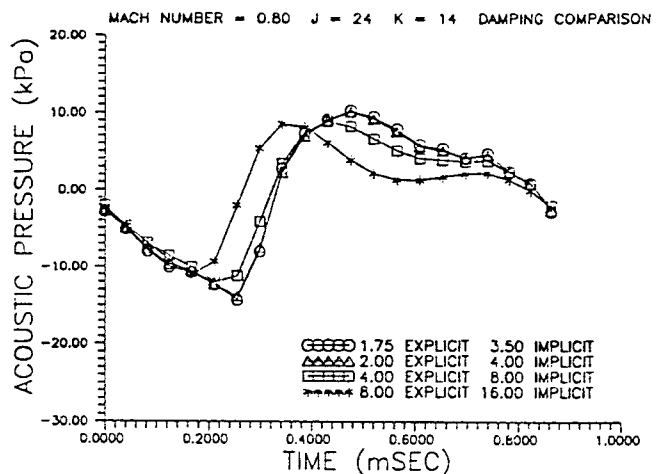


Figure 7. Acoustic Pressure Time-Histories for Different Damping Values. $r/R_{tip} = 1.08$ $z/R_{tip} = 0.25$

Since the areas far from the blade have greater mesh spacing than the region near the blade tip, and the local damping is scaled to the local time step size, the effect of the damping increases as the observer moves away from the blade radially. It is seen from the acoustic pressure time histories, that the effect of this scaling is to overdamp most of the region used in acoustic calculations. However from the Mach contours on the propeller surface at $K=11$, it is apparent that there is insufficient damping in the lower damping cases as seen in Figs. 9-12. The dilemma the user faces is that the optimum damping for acoustic analyses is not necessarily the best damping for flowfield analyses on the propeller

blade surfaces.

The incompatibility of the damping values is directly related to the problem of proper distribution of grid points. If the grid points were more equally spaced, the variation of the scaling of the damping would not be as great. Then the minimum damping required to eliminate dispersive waves in the solution would produce the best results in both the blade surface and acoustic regions of the flow field. A more expedient solution may be to modify the scaling of the damping coefficients to reduce their effect on the coarse regions of the mesh, but this approach would add complexity to the flow field solution scheme and may cause problems with obtaining a unique solution if the scaling of the damping must be user specified. Generally, the number of user defined parameters not directly related to the physical conditions to be modelled should be minimized. In the near field method those parameters are the damping factors, Courant number, and the grid. In the far field method, the radius of the control cylinder used for the surface integration is the primary user specified parameter that could affect the acoustic solution.

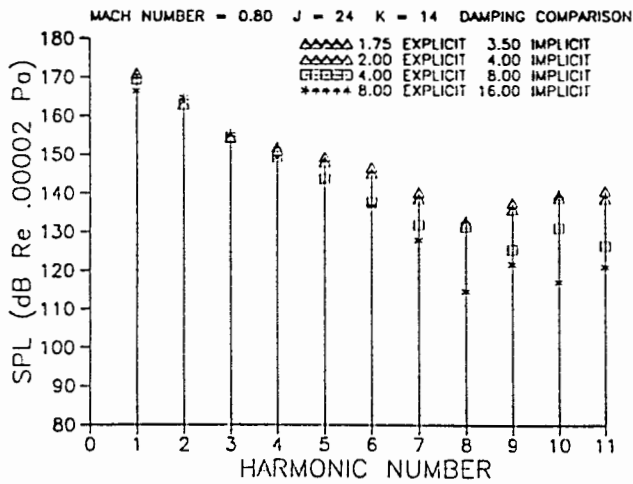


Figure 8. Frequency Spectra for Different Damping Values.
 $r/R_{tip} = 1.08$ $z/R_{tip} = 0.25$

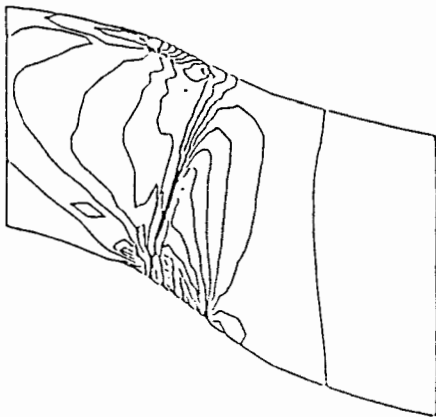


Figure 9. IsoMach Contours for 1.75/3.50 Damping.
 $z/R_{tip} = 0.98$

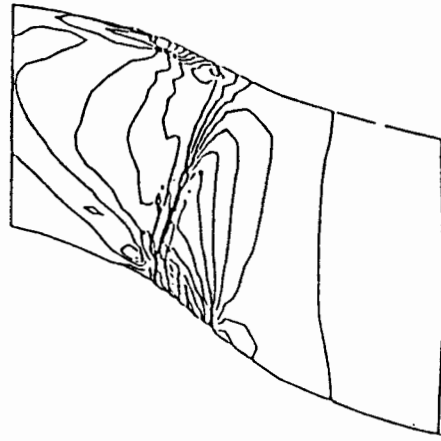


Figure 10. IsoMach Contours for 2.00/4.00 Damping.
 $z/R_{tip} = 0.98$

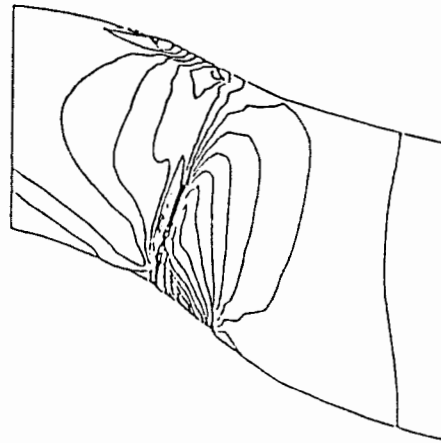


Figure 11. IsoMach Contours for 4.00/8.00 Damping.
 $z/R_{tip} = 0.98$

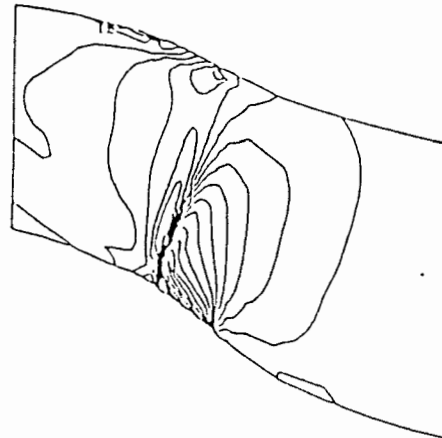


Figure 12. IsoMach Contours for 8.00/16.0 Damping.
 $z/R_{tip} = 0.98$

Determination of Far Field Acoustics

The far field as defined here, include those areas outside the computational domain of the three dimensional flow field solver which include all non-linear behavior such as shock waves and steep gradients. A complete understanding of far field acoustics will lead to better predictions of aircraft takeoff noise, sideline noise, and flyover noise resulting from propellers.

Modern methods of solving the problem of high speed propeller acoustics have been based on Lighthill's acoustic analogy¹. A common form of Lighthill's acoustic analogy is that developed by Ffowcs Williams and Hawkings²:

$$4\pi a_o^2(\rho - \rho_o)(\underline{x}, t) = \frac{\partial}{\partial t} \int \left[\frac{\rho_o V_n}{r|1 - M_r|} \right] dS - \frac{\partial}{\partial x_i} \int \left[\frac{P_{ij} n_j A}{r|1 - M_r|} \right] dS + \frac{\partial^2}{\partial x_i \partial x_j} \int \left[\frac{T_{ij}}{r|1 - M_r|} \right] dV \quad (5)$$

where the three terms on the right hand side of Equation (5) are the thickness, loading, and quadrupole noise sources, respectively. When applying Lighthill's analogy, problems are encountered with the specification of the quadrupole field and determination of its effects on acoustic characteristics. It is unlikely that the quadrupole term can be approximated independently of the acoustic field that it generates.

In linear theory, the quadrupole term is neglected. Difficulty arises with Equation (5) in that sonically rotating sources can lead to singularities in the acoustic waveform. Thus it makes it difficult to evaluate the quadrupole term in the time domain. Alternate methods have been developed that yield the acoustic far field from near field information without a direct evaluation of the quadrupole field.

Previously, the approach has been to use a method proposed by Hawkings²⁸. The Hawking's approach uses Kirchoff's theorem applied to a nonrotating system such as a helicopter main rotor blade. The acoustic pressure can be obtained at any far field location by applying the method to near field acoustic information on the control surface. This includes the total pressure and its spatial derivatives obtained numerically from a three dimensional flow field solver. The method is described by the following equation:

$$\Phi(\underline{x}, t) = \frac{-1}{4\pi} \iint_c \left[\frac{1}{R} \frac{\partial \Phi}{\partial n} + \frac{1}{a_o R} \frac{\partial R}{\partial n} \frac{\partial \Phi}{\partial \tau} - \frac{\Phi}{R^2} \frac{\partial R}{\partial n} \right] dc \quad (6)$$

A cylinder, concentric with the axis of the engine, is used as the nonrotating control surface. The control surface also includes two disks at each end of the cylinder. The radius of the control surface, b , must be large enough to enclose all of the non-linear phenomena such as shock waves and/or steep gradients associated with the rotating system. This assumes then that the linear

wave equation can be applied outside the domain of the control cylinder. The control cylinder can not be made too large since the numerical solutions lose accuracy due to lack of resolution far from the blade tip.

Hawkings notes that the last term in Equation (6) is a near field term and can be dropped in the far field. If cylindrical coordinates, concentric with C , are adopted as shown in Fig. 13, Equation (6) becomes:

$$\Phi(\underline{x}, t) = -\frac{b}{4\pi R_o} \iint_c \left[\frac{\partial P}{\partial b} - \frac{\Omega}{a_o} \frac{\partial R}{\partial b} \frac{\partial P}{\partial \psi} \right] d\psi dz \quad (7)$$

With this Equation, the acoustic pressure at far field locations can be determined in the time domain. It

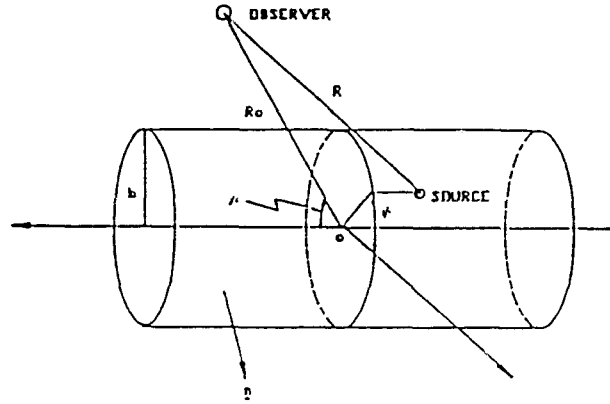


Figure 13. Control Cylinder Coordinate System.

was found that the method, when evaluated in the time domain, required a relatively fine grid in order that the spatial derivatives of the pressures on the control surface can be resolved. Hawkings further developed his method to express the acoustic pressure as a harmonic series in the frequency domain by transforming Equation (6) with a Fast Fourier Transform (FFT). This results in

$$\Phi(t) = \sum_{m=-\infty}^{\infty} C_m \exp\{-im[\Omega(t - R_o/a_o - \nu)]\} \quad (8)$$

where,

$$C_m = -\frac{b}{2R_o} \exp\left\{-im\frac{\pi}{2}\right\} \cdot \int_{-\infty}^{\infty} \exp\left\{-\left(im\frac{\Omega z}{a_o}\right) \cos \mu\right\} \cdot \left[\left(\frac{\partial \Phi}{\partial b}\right)_m(z) J_m\left(m\frac{\Omega b}{a_o} \sin \mu\right) - \Phi_m(z) \frac{\partial J_m}{\partial b}\left(m\frac{\Omega b}{a_o} \sin \mu\right) \right] dz$$

The Fourier coefficient of $\Phi(z, \psi - \Omega\tau)$ with respect to $(\psi - \Omega\tau)$ is $\Phi_m(z)$ and is defined by,

$$\Phi(z, \psi - \Omega\tau) = \sum_{-\infty}^{+\infty} \Phi_m(z) e^{im(\psi - \Omega\tau)} \quad (9)$$

Sound pressure level can then be obtained at different harmonic numbers. Overall sound pressure level can be determined at different radial distances which will result in the characteristic "roll off" as shown in Fig. 14.

If the propeller configuration is at an angle of attack of zero, a flow field solver can simplify the problem of creating a three dimensional flow field by determining the pressure field between two blades and assuming periodicity. The pressure and the time and normal derivatives of the pressure are periodic over the surface, therefore only the acoustic pressure between two blades is used to determine the full three dimensional aerodynamic near field. The far field acoustic pressure depends on the total contribution from the entire cylinder and the two disks. The distances from each blade to the far field observation point will be different at a fixed observer time.

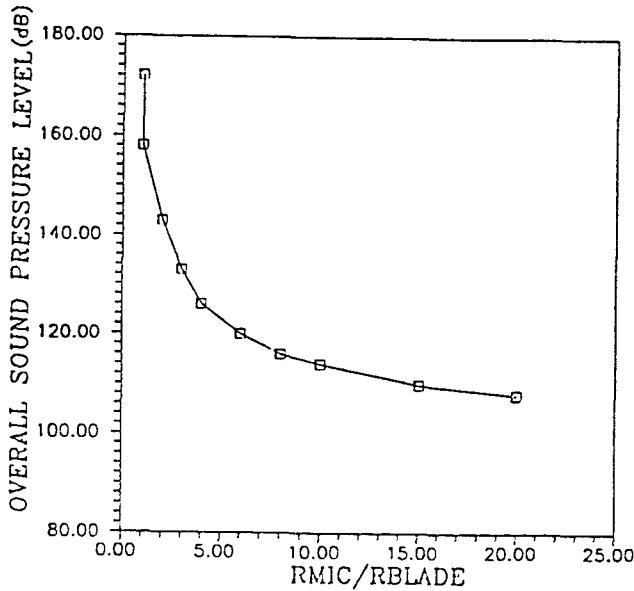


Figure 14. Overall Sound Pressure Level v.s. Ratio of Observer to Blade Distance.

Hawking developed his method for helicopter main rotor blades that are stationary or translating at low speeds. It was found that Hawking's method did not adequately predict the far field acoustics resulting from high speed propellers translating at transonic Mach numbers. A new approach presently being investigated, is to apply a method outlined by Farassat and Myers³⁰. Using generalized functions, Farassat and Myers developed a general version of Hawking's method for control surfaces which are in motion with respect to

the ambient fluid. This method will account for the effects of forward motion as well as the non-linear effects that are evident in the near field computational solution. This method should then be applicable to high speed propellers operating at transonic Mach numbers such as the NASA SR series. The solution is expressed by the following equation:

$$\Phi(\underline{x}, \tau) = \frac{1}{4\pi} \iint_c \left[\frac{E_1}{r(1-M_r)} \right]_{ret} dc + \frac{1}{4\pi} \iint_c \left[\frac{\Phi E_2}{r^2(1-M_r)} \right]_{ret} dc \quad (10)$$

where,

$$E_1 = (M_n^2 - 1)\Phi_n + M_n \dot{M}_t \cdot \nabla_2 \Phi - \frac{M_n \dot{\Phi}}{a_o} + \frac{1}{a_o(1-M_r)} \left[(\dot{n}_r - \dot{M}_n - \dot{n}_M)\Phi + (\cos\theta - M_n)\dot{\Phi} + (\cos\theta - M_n)\Phi\dot{\sigma} \right] + \frac{1}{a_o(1-M_r)^2} \left[\dot{M}_r(\cos\theta - M_n)\Phi \right]$$

and,

$$E_2 = \cos\theta + \frac{1}{1-M_r} \left[2M_r \cos\theta - M_n M_r - M_n \right] + \frac{1}{(1-M_r)^2} \left[(\cos\theta - M_n)(M_r^2 - M^2) \right]$$

Equation (10) can be further simplified by assuming a rigid control surface and a zero angle-of-attack for the engine. Since the engine is not accelerating, the time derivatives of the mach number components, \dot{M}_n , \dot{M}_r , and the surface normal components, \dot{n}_M, \dot{n}_r will all be zero. The normal component of Mach number, M_n will be zero on the cylinder surface and equal to the Mach number on the disks. The tangential component of Mach number, \dot{M}_t will be zero on the disks and equal to the Mach number on the cylinder. This results in the following:

$$\Phi(\underline{x}, \tau) = \frac{1}{4\pi} \iint_c \left[\frac{E_1}{r(1-M_r)} \right]_{ret} dc - \frac{1}{4\pi} \iint_c \left[\frac{\Phi E_2}{r^2(1-M_r)} \right]_{ret} dc \quad (11)$$

where,

$$E_1 = (M_n^2 - 1)\Phi_n - \frac{M_n \dot{\Phi}}{a_o} - \frac{1}{a_o(1-M_r)} \left[(\cos\theta - M_n)\Phi \right]$$

and,

$$E_2 = \cos\theta + \frac{1}{1-M_r} \left[2M_r \cos\theta - M_n M_r - M_n \right] - \frac{1}{(1-M_r)^2} \left[(\cos\theta - M_n)(M_r^2 - M^2) \right]$$

In Hawking's approach it was shown that Equation (6) could be evaluated directly in the frequency domain by transforming the Equation by utilization of the FFT. Since the complexity of the Farassat and Myer's approach makes it impractical to transform Equation (10) with an FFT, the equation will be evaluated numerically in the time domain. This will reveal the acoustic characteristics of the propeller system at different times between each blade passage. Then an FFT will be applied to the results to obtain the sound pressure level in the frequency domain.

The Hawking's method has been programmed to provide results in the time domain. Results will be compared to those obtained for the frequency domain. The Farassat and Myer's equation has also been programmed to provide results in the time domain. The results will then be compared to the time and frequency results obtained from the Hawking's method.

The accuracy of applying Kirchhoff's formula to an acoustic far field problem can be tested by placing a single point source within the control cylinder instead of a propeller as shown in fig. 15. This source would supply the local acoustic pressure and its time and normal derivatives on the surface. This in turn would be the near field information needed for the Kirchhoff's formulation.³¹

Each method will be evaluated with and without the $1/R^2$ term present in Equations 6 and 10. Results obtained by using different control cylinder radii will also be compared to determine the relationship between control surface size and accuracy in the far field. Both methods will be used in conjunction with several three dimensional flow field solvers such as those developed by Bober et al.^{21,22}, Celestina et al.³² and Denton³³. The results from both methods will be compared to experimental data obtained from the SR-3 and UDF propeller configurations when made available.

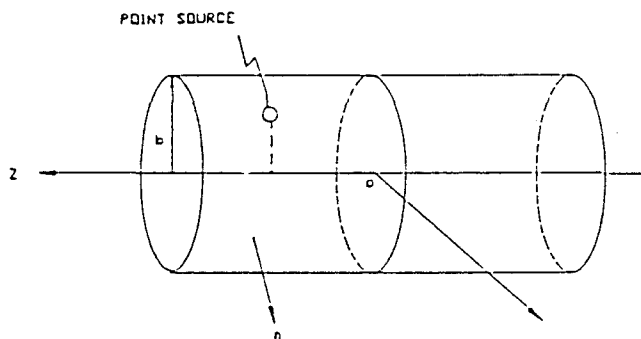


Figure 15. A Point Source Inside Control Volume.

Summary

A method of predicting acoustic data from the non-linear flow field generated by an Euler solver has been demonstrated. A variety of different computational conditions were employed to test the limitations of the Euler solution method(s) and demonstrate how these limitations reflect on the quality of results of the acoustic calculations in the near field. It was shown that the effects of mesh spacing has a significant effect on the Euler solution which is manifested in the acoustic pressure time-histories and frequency spectra predicted in the near field. It has also been shown that reducing the reflectiveness of the boundaries used to simulate free stream conditions slightly reduced the noise levels predicted in the near field. In addition the effects of numerical damping on the solutions of the flow field and predictions of the acoustic near field showed that it was possible to distort the acoustic pressure time history by excessive numerical dissipation in the regions of the domain that are far from the blade.

The numerical dissipation caused unexpected phase shifts in the pressure time histories as well as spurious waves resulting from the scaling of the local damping coefficients to the local time step size. This problem is related to the non-uniform spacing of grid points in the computational domain and can be resolved by using either a more adaptable distribution of artificial viscosity or a more uniform mesh. The results of this study show that boundary reflections do not pose serious problems in the use of the Euler solution for acoustic analysis. The reflected waves were extremely small in amplitude and were restricted to the outermost segment of the grid, which would not typically be used for practical acoustic analysis.

The most significant problem in the use of this method is the generation of the computational mesh used in the flowfield analysis. First, the true geometry of the SR-3 propeller during actual operation has not been accurately determined. The SR-3 undergoes dynamic untwist under centrifugal and aerodynamic loading. However, the geometry must be known to obtain the aerodynamic loads, but the structural loading must be known to obtain the propeller geometry. In this study the blade was pitched as a rigid body so that the 75 % radial station was untwisted by 3.4° from the unloaded blade angle of 61.3° . It is believed that the tip region geometry will be close to the experimental data, but the region near the hub becomes negatively loaded using this approach. Second, the distribution of grid points in the azimuthal planes must be optimized further. The grid smoothing routine only partially alleviates the distortion of the acoustic field due to grid point clustering in the acoustic near field. It may be necessary to add more radial stations beyond the blade tip, while keeping the freestream boundary in the same location relative to the blade. Third, the grid resolution direction still may be insufficient to obtain good acoustic data for the higher harmonics of the blade passing

frequency.

In conclusion, the method used in this study is more efficient than solutions of the Ffowcs-Williams Hawkins equation if acoustic data is needed for a large number of near and far field observer locations. The present solution method may be improved by using flow data generated by a different flow field solver which is currently under study as is the far field method²⁴. Previous comparisons²⁵ of the present acoustic method with overall experimental acoustic data of the SR-3 propfan have yielded acceptable results. However, present efforts are needed which will provide greater acoustic detail such as more refined near field acoustic time histories and frequency spectra.

Acknowledgment

This research was supported by NASA Lewis Research Center Grant NAG 3-354.

References

1. Lighthill, M.J., "On Sound Generated Aerodynamically; I. General Theory, II. Turbulence as a Source of Sound," *Proceeding of the Royal Society of London*, A221, (1952) and A222, (1954).
2. Ffowcs Williams, J.E. and Hawkins, D.L., "Sound Generated by Turbulence and Surfaces in Arbitrary Motion," *Philosophical Transactions of the Royal Aeronautical Society of London*, Vol. A264, (1969).
3. Farassat, F., "Linear Acoustic Formulas for Calculation of Rotating Blade Noise," *AIAA Journal*, Vol. 19, (1981), pp. 1122-1130.
4. Lynam, E.J.H. and Webb, H.A., "The Emission of Sound by Airscrews," *R.&M. No. 624*, British A.C.A., (1919).
5. Hart, M.D., "The Aeroplane as a Source of Sound," *R.&M. No. 1310*, British A.R.C., (1930).
6. Gutin, L., "On the Sound Field of a Rotating Propeller," *NACA TM 1195*, 1948. (From *Phys. Zeitschr. der Sowjetunion*, Band 9, Heft 1, 1936, pp. 57-71).
7. Hubbard, H.H. and Regier, A.A., "Free-Space Oscillating Pressures Near the Tips of Rotating Propellers," *NACA Rep. 996*, (1950).
8. Garrick, I.E. and Watkins, C.E., "A Theoretical Study of the Effect of Forward Speed on the Free-Space Sound Pressure Field Around Propellers," *NACA TM 3018*, (1953).
9. Hawkins, D.L. and Lawson, M.V., "Theory of Open Supersonic Rotor Noise," *Journal of Sound and Vibration*, Vol. 36, (1974), pp. 1-20.
10. Jou, W.H., "Supersonic Propeller Noise in a Uniform Flow," *AIAA Paper 79-0348*, (1979).
11. Farassat, F., "Theory of Noise Generation from Moving Bodies with an Application to Helicopter Rotors," *NASA TR-451*, (1975).
12. Farassat, F. and Succi, G.P., "A Review of Propeller Discrete Frequency Noise Prediction Technology with Emphasis on Two Current Methods for Time Domain Calculations," *Journal of Sound and Vibration*, Vol. 71, (1980), pp. 399-419.
13. Nystrom, P.A. and Farassat, F., "A Numerical Technique for Calculation of the Noise of High Speed Propellers with Advanced Geometry," *NASA TP 1662*, (1980).
14. Farassat, F., "Quadrupole Source in Prediction of the Noise of Rotating Blades - A New Source Description," *AIAA Paper No. 87-2675*, (1987).
15. Hanson, D.B., "Near Field Noise of High Tip Speed Propellers in Forward Flight," *AIAA Paper No. 76-565*, (1976).
16. Hanson, D.B., "Near Field Frequency - Domain Theory for Propeller Noise," *AIAA Paper No. 83-688*, (1983).
17. Woan, C.J. and Gregorek, G.M., "The Exact Numerical Calculation of Propeller Noise," *AIAA Paper No. 78-1122*, (1978).
18. Woan, C.J., Gregorek, G.M., and Korkan, K.D., "Acoustic Evaluation of Three Turbo Propellers," *SAE Paper No. 830733*, (1983).
19. Succi, G.P., "Design of Quiet Efficient Propellers," *SAE Paper No. 790584*, (1979).
20. Hanson, D.B. and Fink, M.R., "The Importance of Quadrupole Sources," Paper presented to the Spring Meeting of the Institute of Acoustics, Cambridge University, Cambridge, England, (1978).
21. Bober, L.J., Chausee, D.S. and Kutler, P., "Prediction of High Speed Propeller Flow Fields Using a Three-Dimensional Euler Analysis," *NASA TM 83065*, (1983).
22. Barton, J.M., Yamamoto, O., and Bober, L.J., "Inviscid Analysis of Advanced Turboprop Propeller Flow Fields," *AIAA Paper No. 85-1263*, (1985).
23. White, T.A., "Numerical Evaluation of Propeller Noise, Including Non-Linear Effects," Thesis, Texas A&M University, (1984).
24. Korkan, K.D., von Lavante, E. and White, T.A., "An Alternative Method of Calculating Propeller Noise Generated at Transonic Tip Speeds. Including Non-Linear Effects," *AIAA Paper No. 85-0002*, (1985).
25. Korkan, K.D., von Lavante, E. and Bober, L.J., "Numerical Evaluation of Propeller Noise Including Non-Linear Effects," *AIAA Journal*, Vol. 24, (1986), pp. 1043-1045.
26. Dittmar, J.H., Jeracki, R.J. and Blaha, B.J., "Tone Noise of Three Supersonic Helical Tip Speed Propellers in a Wind Tunnel," *NASA TM 79167*, (1979).
27. Dittmar, J.H. and Jeracki, R.J., "Additional Noise Data on the SR-3 Propeller," *NASA TM 81736*, (1981).
28. Hawkins, D.L., "Noise Generated by Transonic Open Rotors," *Research Paper No. 599*, Westland Helicopters Limited, (1979).
29. Hawkins, D.L., Personal Correspondence, (May 1986).

30. Farassat, F. and Myers, M.K., "Extension of Kirchhoff's Formula to Radiation From Moving Surfaces," NASA TM 87149, (1987).
31. Farassat, F., Personal Interview, (March 1989).
32. Celestina, M.L., Mulac, R.A., and Adamczyk, J.J., "A Numerical Simulation of the Inviscid Flow Through a Counterrotating Propeller," ASME Paper No. 86-GT-138, (Jan. 1986).
33. Denton, J.D. and Singh, U.K., "Time Marching Methods for Turbomachinery Flow Calculation," (April 1979).